Chinese Journal of Natural Medicines

DeepGCGR: an interpretable two-layer deep learning model for the discovery of GCGR-activating compounds

Xinyu Tang, Hongguo Chen, Guiyang Zhang, Huan Li, Danni Zhao, Zenghao Bi, Peng Wang, Jingwei Zhou, Shilin Chen, Zhaotong Cong, Wei Chen

Citation: Xinyu Tang, Hongguo Chen, Guiyang Zhang, Huan Li, Danni Zhao, Zenghao Bi, Peng Wang, Jingwei Zhou, Shilin Chen, Zhaotong Cong, Wei Chen, DeepGCGR: an interpretable two-layer deep learning model for the discovery of GCGR-activating compounds, Chinese Journal of Natural Medicines, 2025, 23(11), 1301-1309. doi: 10.1016/S1875-5364(25)60969-1.

View online: https://doi.org/10.1016/S1875-5364(25)60969-1

Chinese Journal of Natural Medicines 23 (2025) 1301-1309

Contents lists available at ScienceDirect

Chinese Journal of Natural Medicines

journal homepage: www.cjnmcpu.com/

Original article

DeepGCGR: an interpretable two-layer deep learning model for the discovery of GCGR-activating compounds

Xinyu Tang[a,Δ], Hongguo Chen[b,Δ], Guiyang Zhang[c,d], Huan Li[e], Danni Zhao[a], Zenghao Bi[e], Peng Wang[e], Jingwei Zhou[e], Shilin Chen[d,e], Zhaotong Cong[d,e,*], Wei Chen[d,e,*]

[a] School of Intelligent Medicine, Chengdu University of Traditional Chinese Medicine, Chengdu 611137, China
[b] State Key Laboratory of Quality Research in Chinese Medicine, Institute of Chinese Medical Sciences, University of Macau, Macau 999078, China
[c] School of Basic Medicine, Chengdu University of Traditional Chinese Medicine, Chengdu 611137, China
[d] Innovative Institute of Chinese Medicine and Pharmacy, Chengdu University of Traditional Chinese Medicine, Chengdu 611137, China
[e] Institute of Herbgenomics, Chengdu University of Traditional Chinese Medicine, Chengdu 611137, China

ARTICLE INFO

Article history:
Received 23 April 2025
Revised 12 May 2025
Accepted 15 August 2025
Available online 20 November 2025

Keywords:
Artificial intelligence
Deep learning
Type 2 diabetes mellitus
G protein-coupled receptor
Natural products

ABSTRACT

The glucagon receptor (GCGR) is a critical target for the treatment of metabolic disorders such as Type 2 Diabetes Mellitus (T2DM) and obesity. Activation of GCGR enhances systemic insulin sensitivity through paracrine stimulation of insulin secretion, presenting a promising avenue for treatment. However, the discovery of effective GCGR agonists remains a challenging and resource-intensive process, often requiring time-consuming wet-lab experiments to synthesize and screen potential compounds. Recent advances in artificial intelligence technologies have demonstrated great potential in accelerating drug discovery by streamlining screening and efficiently predicting bioactivity. In the present work, we propose DeepGCGR, a two-layer deep learning model that leverages graph convolutional networks (GCN) integrated with a multiple attention mechanism to expedite the identification of GCGR agonists. In the first layer, the model predicts the bioactivity of various compounds against GCGR, efficiently filtering large chemical libraries to identify promising candidates. In the second layer, DeepGCGR classifies high bioactive compounds based on their functional effects on GCGR signaling, identifying those with potential agonistic or antagonistic effects. Moreover, DeepGCGR was specifically applied to identify novel GCGR-regulating compounds for the treatment of T2DM from natural products derived from traditional Chinese medicine (TCM). The proposed method will not only offer an effective strategy for discovering GCGR-targeting compounds with functional activation properties but also provide new insights into the development of T2DM therapeutics.

1. Introduction

Type 2 Diabetes Mellitus (T2DM), accounting for nearly 90% of diabetes cases globally, affects an estimated 537 million individuals and poses a major global health challenge [1]. T2DM is characterized by elevated blood glucose levels due to insulin resistance in target cells combined with insufficient insulin secretion [2]. Persistent hyperglycemia can cause microvascular damage, leading to complications such as diabetic nephropathy, retinopathy, and neuropathy [3, 4].

Numerous pharmaceuticals have been utilized for managing T2DM, including insulin, biguanides, insulin secretagogues, thiazolidinediones, and other types of drugs [5, 6]. Insulin and its analogs are the cornerstone of diabetes treatment, functioning as a key regulator of blood glucose, lipid, and protein metabolism to maintain glucose homeostasis and effectively control the disease [7]. Metformin, a widely used biguanide, serves as the first-line therapy for T2DM by suppressing hepatic gluconeogenesis and activating AMP-activated protein kinase (AMPK), thereby enhancing insulin sensitivity [8]. Thiazolidinediones, another class of antidiabetic agent, activate peroxisome proliferator-activated receptor gamma (PPAR-γ) and enhance PPAR signaling in skeletal muscle, thereby mitigating insulin resistance and improving insulin responsiveness in individuals with T2DM [9]. Agonists of the glucagon-like peptide-1 receptor (GLP-1R), commonly employed as insulin secretagogues, exert their effects by binding to GLP-1R and promoting insulin secretion through activating protein kinase A (PKA) or stimulating cyclic AMP (cAMP) signaling pathways [10]. Although GLP-1 based therapies have demonstrated significant efficacy in lowering glycated hemoglobin (HbA1c), their dose-dependent adverse effects have limited the clinical use of higher doses [11]. Preclinical studies have shown that incorporating glucagon receptor (GCGR) agonists with GLP-1R agonists, or even combining the three agonists for GCGR, GLP-1R, and glucose-dependent insulinotropic polypeptide receptor (GIPR), into a single molecule can significantly enhance therapeutic outcomes [12-14]. Moreover, these dual or triple agonists have maintained

* Corresponding author.
E-mail addresses: congzt@cdutcm.edu.cn (Z. Cong); greatchen@ncst.edu.cn (W. Chen)
Δ These authors contributed equally to this work.

https://doi.org/10.1016/S1875-5364(25)60969-1

high efficacy while offering a more favorable efficacy-safety profile [15]. Consequently, the use of combination regimens has become a prevalent clinical practice in T2DM management [16].

While combination therapies involving GCGR agonists have shown promising clinical benefits, the discovery of novel and selective GCGR agonists remains crucial to fully harness the therapeutic potential of this receptor. As a member of the GPCR family, GCGR regulates glucose homeostasis through its interaction with glucagon [17]. Upon glucagon binding, GCGR activates G proteins, leading to cAMP production that promotes hepatic glycogen breakdown and subsequently elevates blood glucose concentrations [18]. Under both hyperglycemic and normoglycemic conditions, GCGR activation has been shown to enhance systemic insulin sensitivity [19]. Glucagon also exerts paracrine effects by stimulating insulin secretion *via* activation of β-cell GCGR and GLP-1R [20], a synergistic mechanism that can be reproduced by coupling GCGR agonists with existing insulin secretagogues [21]. Moreover, GCGR agonism not only alleviates metabolic dysfunction-associated steatotic liver disease (MASLD) and metabolic dysfunction-associated steatohepatitis (MASH), but also improves insulin sensitivity and activates brown adipose tissue *via* dual GLP-1R/GCGR agonism, thereby reducing insulin requirements and facilitating the functional restoration of β-cells [22]. Consequently, discovering and developing novel GCGR modulators, including both orthosteric agonists and positive allosteric modulators (PAMs), holds substantial promise as an innovative therapeutic strategy for diabetes.

In addition to modern medicine, traditional Chinese medicine (TCM) provides unique benefits for managing T2DM. Through its multi-mechanistic pharmacological effects, TCM can reduce reliance on conventional medications and mitigate diabetes-related complications [23]. TCM formulas, which are integral to TCM, contain a large number of ingredients, most of which are natural products. A recent review demonstrated that at least 16 FDA-approved drugs targeting GPCRs are derived from natural products or their derivatives [24]. These natural products are chemically diverse and multi-targeted [25], making them an excellent resource for screening GCGR targeting compounds for T2DM treatment. However, conventional experimental approaches in drug development remain resource-intensive and time-consuming [26]. Artificial Intelligence (AI), with its advanced data analysis and pattern recognition capabilities, has emerged as a transformative tool in drug discovery. By screening and analyzing extensive chemical libraries, AI algorithms can quickly identify drug molecules with potential activity, thereby improving development efficiency of drug development and reducing costs [27, 28]. For instance, Mizera et al. developed a QSAR model for predicting the pEC_{50} values of GLP-1R compounds and the pIC_{50} values of GCGR compounds, providing a methodology for identifying potential dual-action compounds [29]. Similarly, Puszkarska et al. designed a novel GCGR/GLP-1R dual agonist using a deep multitask neural network, demonstrating the potential of AI in drug discovery [30].

Inspired by these works, we presented DeepGCGR, a two-layer deep learning model that integrates graph-based feature representations with Graph Attention Network (GAT) and Graph Convolutional Network (GCN) architectures to predict compounds with potential agonistic activity toward GCGR. To enhance interpretability, we conducted feature attribution analyses to identify key chemical properties and structural motifs driving the model's predictions, thereby elucidating its decision-making process. Leveraging DeepGCGR, we screened a natural product library and identified candidate compounds with agonistic activity. One top-ranked candidate was subsequently validated experimentally and, notably, found to function as a PAM of GCGR. All source code and datasets for DeepGCGR are publicly available at https://github.com/GreatChenLab/DeepGCGR.

2. Materials and methods

2.1. Benchmark datasets

The datasets used for the GCGR compound activity prediction model (P-model) and the GCGR compound classification model (C-model) were obtained from the GPCRdb database (https://gpcrdb.org/) [31]. The data collection process is depicted in Fig. 1A. Compounds with SMILES (Simplified Molecular Input Line Entry System) for human GPCR were retrieved using the keyword "<id>_human". In the data cleaning phase, duplicate entries were removed based on their SMILES. Subsequently, the dataset was standardized using RDKit (http://www.rdkit.org/) by transforming SMILES into isomeric SMILES representations. Non-GCGR compounds and those lacking IC_{50}, EC_{50}, or K_i values were removed, resulting in a final dataset (GCGR_P) of 1 708 compounds. For the C-model, compounds without agonist/antagonist labels were excluded.The resulting dataset (GCGR_C) was composed of a pre-training dataset and a fine-tuning dataset. The pre-training dataset contained 37,764 compounds targeting GPCRs other than GCGR, including 20,112 agonists and 17,652 antagonists, while the fine-tuning dataset consisted of 53 agonists and 270 antagonists targeting GCGR.

2.2. Model construction

2.2.1. Feature representation

Each molecule in the dataset was represented as a molecular graph [32] (Fig. 1B). In the molecular graph, atoms and edges are defined by feature $\boldsymbol{v} \in \{0,1\}^{78}$ and $\boldsymbol{e} \in \{i,j\}^2$ using RDkit (http://www.rdkit.org/), respectively. The elements in $\boldsymbol{v}$ is the presence (indicated by 1) or absence (indicated by 0) of the 78 atomic features (Table S1). The elements in $\boldsymbol{e}$ indicate the atom-to-atom relationships, the first one is the index of the starting atom i and the second is that of target atom j. Accordingly, the atom feature matrix $V \in \{0,1\}^{n_v \times 78}$ and edge indices matrix $E \in \{i,j\}^{n_e \times 2}$ can be obtained, with n_v indicating the total count of atoms and n_e signifying the number of edges. Finally, the PyTorch Geometric library was employed to convert these two matrices into tensors.

2.2.2. Graph attention network (GAT) layer

We constructed the GAT using CustomGATConv, which is a variant of GATConv that allows for flexible model configuration. The GAT layer integrates a multi-head attention mechanism to compute attention weights between neighboring features. The attention score between node i and its neighbor j is calculated as follows:

$$e_{ij} = \mathrm{LeakyReLU}\left(a^T\left[Wh_i \,||\, Wh_j\right]\right) \tag{1}$$

where h_i and h_j denote the input feature vectors for nodes i and j, respectively. The calculation involves a linear transformation (W), a vector concatenation operation (||), and a learnable attention weight vector (a). LeakyReLU is used as the activation function for the process to mitigate the issue of "dead neurons".

The attention scores for neighbors are normalized using the Softmax function:

$$a_{ij} = \mathrm{softmax}_j(e_{ij}) = \frac{\exp(e_{ij})}{\sum_{k \in N_i} \exp(e_{ik})} \tag{2}$$

N_i is the set of neighbors of node i, The exponential function exp (·) is applied to the attention scores to transform them into non-negative values, which amplifies the relative importance of higher scores.

GAT employs multiple independent attention heads to learn diverse attention distributions. Each attention head has its own

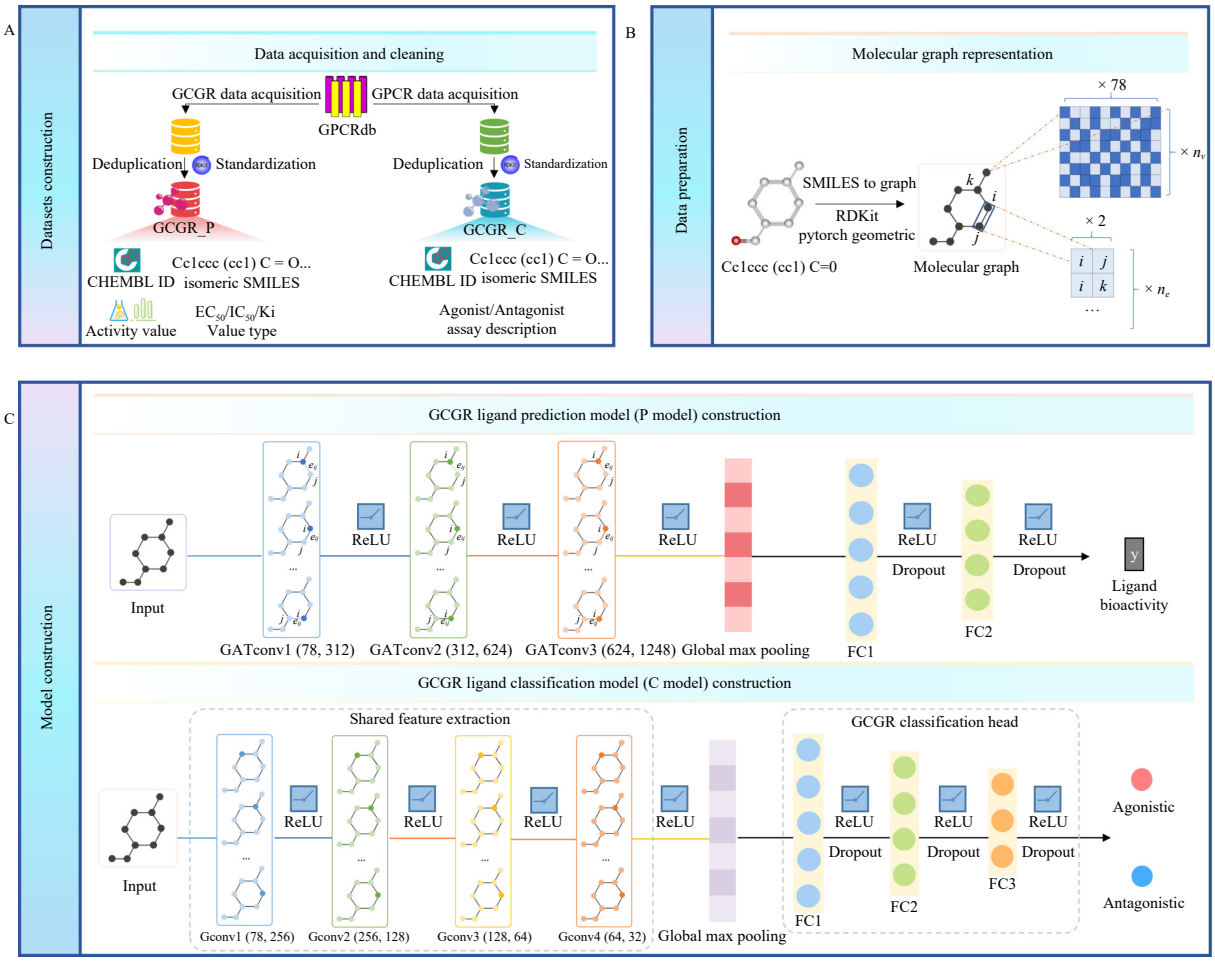

Fig. 1 Architecture of DeepGCGR. (A) Construction of the GCGR compound activity prediction model dataset and the GCGR compound classification model dataset. (B) Scheme of feature representation. (C) Development of the GCGR compound activity prediction model and the GCGR compound classification model. The molecular graph edge weights in the GAT layers were computed using $e_{ij} = \mathrm{LeakyReLU}\left(a^T[Wh_i \,||\, Wh_j]\right)$.

weight matrix W^k and computes an attention coefficient $a_{ij}^{(k)}$. The output representation of node i from the k-th attention head is computed as:

$$h_i^{(k)} = \sigma\left(\sum_{j \in N(i)} a_{ij}^{(k)} W^k h_j\right) \tag{3}$$

where $N(i)$ represents the set of neighbors of node i, h_j is the feature vector of neighbor node j, and W^k represents the trainable weight matrix corresponding to the k-th attention head. σ stands for an activation function. The ReLU [33] was used as the activation function to construct the P-model, defined as:

$$\mathrm{ReLU}(x) = \max(0, x) \tag{4}$$

the output is x when the input x is greater than 0, and the output is 0 when x is less than or equal to 0.

The final feature representation h_i' is obtained by concatenating the outputs of all K attention heads:

$$h_i' = ||_{k=1}^{K} h_i^{(k)} \tag{5}$$

In this study, the number of attention heads K is set to 4.

2.2.3. Graph convolutional network (GCN) layer

We constructed a GCN utilizing GCNConv. The GCN layer employs an update rule based on the aggregation of the adjacency matrix, enabling each node's representation to incorporate both its own features and those of its neighbors. To stabilize training, the adjacency matrix is first normalized as follows:

$$\begin{cases} \tilde{A} = A + I_N \\ \hat{A} = \tilde{D}^{-1/2} \tilde{A} \tilde{D}^{-1/2} \end{cases} \tag{6}$$

where A denotes the symmetric adjacency matrix, I_N represents the identity matrix, and $\tilde{D}$ is the degree matrix of $\tilde{A}$.

The formula for a single-layer GCN is:

$$H^{(l)} = \sigma\left(\hat{A} X W^{(0)}\right) \tag{7}$$

where X is the feature matrix, $W^{(0)}$ is the weight matrix of the first layer.

The formula for a multi-layer GCN is:

$$H^{(l+1)} = \sigma\left(\hat{A} H^{(l)} W^{(l)}\right) \tag{8}$$

where $W^{(l)}$ is the weight matrix of layer l and $H^{(l+1)}$ is the output of layer$l$. σ denotes the activation function. In this study, the C-model was constructed using 4 layers.

2.2.4. Fully connected layer

Following feature extraction by the GCN or GAT layers, node representations were aggregated across the entire graph using global max pooling. The resulting feature vectors were then passed through a series of dense layers to facilitate deeper feature integration and representation learning. To capture complex and nonlinear patterns, each layer was followed by a ReLU activation function. To reduce overfitting, dropout regularization was implemented to randomly discard neurons during training. The P-model outputs the predicted compound activity value from its final fully connected layer, while the C-model outputs classification probability scores from its final layer.

2.2.5. The training processes

During P-model training, a data batch size of 64 was employed. In the three-layer GAT architecture, the output feature di-

mensions for each layer were set to 312, 624, and 1248, respectively. To minimize the mean squared error (MSE), the adaptive moment estimation (Adam) [34] optimizer was applied. Model performance was evaluated using five-fold cross-validation, where the dataset was randomly and evenly divided into five subsets; in each iteration, one subset served as the test set and the remaining four as the training set. This process was repeated for five folds, each trained for 200 epochs. To account for the wide range of GCGR compound potencies, input features were scaled using min–max normalization.

For the C-model training process, separate data partitioning and training strategies were adopted for pre-training and fine-tuning. During pre-training, the GCGR_C dataset was split into training and validation subsets (8 : 2 ratio), using a batch size of 64. For fine-tuning, the GCGR subset was re-split into the same training and test sets using the same ratio, with a reduced batch size of 32. The model architecture comprises a shared feature extraction module of four GCN layers with output dimensions of 256, 128, 64, and 32, respectively. Features obtained after global max pooling are passed to a GCGR-specific classification head and subsequently to the final output layer. We employed the Adam optimizer with a learning rate of 1e-4. For the loss function, we chose nn.BCEWithLogitsLoss, a numerically stable formulation that combines a sigmoid activation with the binary cross-entropy loss. To mitigate overfitting, L2 regularization was introduced with a weight decay coefficient of 1e-4. The model was trained for up to 200 epochs, incorporating an early stopping mechanism that would stop training if performance plateaued. Additionally, the shared GCN layers could be optionally frozen during fine-tuning to exploit pretrained representations. A comprehensive summary of all hyperparameters for both models is provided in Table 1.

Table 1 The hyperparameter values of DeepGCGR during training.

Setting		Attention head	Batch size	Dropout rate	Learning rate	Weight decay
P model		4	64	0.2	1e-4	/
C model	Pre-training	/	64	0.5	1e-4	1e-4
	Fine-tuning	/	32	0.5	1e-4	1e-4

2.3. Model validation

In this study, the evaluation metrics for the P-model include mean squared error (MSE), mean absolute error (MAE), and coefficient of determination (R^2), as defined in equation (9):

$$\begin{cases} \mathrm{MSE} = \frac{1}{n}\sum_{i-1}^{n}(y_i - \hat{y}_i)^2 \\ \mathrm{MAE} = \frac{1}{n}\sum_{i-1}^{n}|y_i - \hat{y}_i| \\ \mathrm{R}^2 = 1 - \frac{\sum_{i=1}^{n}(y_i - \hat{y}_i)^2}{\sum_{i=1}^{n}(y_i - \bar{y})^2} \end{cases} \quad (9)$$

where $\bar{y}$ is the mean of the actual values, y_i is real value, $\hat{y}_i$ is the predicted value, and, n is the number of samples.

The evaluation metrics for the C-model include accuracy (ACC), recall, precision, and F1 score, as defined in equation (10):

$$\begin{cases} \mathrm{ACC} = \frac{TP + TN}{TP + TN + FP + FN} \\ \mathrm{Recall} = \frac{TP}{TP + FN} \\ \mathrm{Precision} = \frac{TP}{TP + FP} \\ \mathrm{F1\ score} = 2 \cdot \frac{Precision \cdot Recall}{Precision + Recall} \end{cases} \quad (10)$$

where TP is the true positive, TN is true negatives, FP is false positives, and FN is false negatives. In addition to these, the C-model evaluates performance using extra metrics, including the area under the precision-recall curve (AUPRC) and the area under the ROC curve (AUROC).

2.4. Molecular docking

Molecular docking simulations were carried out employing the AutoDock Vina [35]. The human GCGR (PDB ID: 4L6R) [36], representing the compound-free (apo) conformation of the receptor, was obtained from the RCSB Protein Data Bank (RCSB PDB) (https://www.rcsb.org/) [37]. Candidate compounds with predicted agonistic effects on GCGR were retrieved from PubChem (https://pubchem.ncbi.nlm.nih.gov/) [38]. The protein structure was prepared using AutoDock Tools (version 1.5.7) by removing water molecules, adding nonpolar hydrogens, and calculating Gasteiger charges. Subsequently, OpenBabel [39] was used to convert the molecular structures into the convenient pdbqt format.

2.5. In vitro cellular assays for GCGR activation

Phorbol 12-myristate 13-acetate (PMA) was purchased from MedChemExpress (compound purity >90%), and glucagon (GCG) was obtained from Shanghai Apeptide Co., Ltd. Cells were seeded in 96-well plates at a density of 35 000 cells per well in 100 μL of medium. Upon 80%–90% confluence, cells were co-transfected with the GCGR-expressing vector and a luminescent cAMP biosensor (GloSensor, Promega) using Lipofectamine 3000 reagent (Thermo Fisher Scientific). After 24 hours transfection, cells were incubated with 80 μL of equilibration medium containing 2% (*V/V*) GloSensor cAMP reagent for 90 minutes at 37 °C. Subsequently, experimental treatments were applied: cells were incubated with 10 μL of test compounds for 30 minutes at room temperature. Ten baseline points for each well were measured before the addition of GCG in a final assay volume of 100 μl, and GCG-induced changes in bioluminescence measurements were then obtained for additional 30 min. Luminescence signals were measured using a BioTek Synergy Neo2 microplate reader (Agilent). Statistical analyses and graphical presentations were performed using GraphPad Prism 10 (GraphPad Software, Inc., San Diego, CA, USA).

3. Results

3.1. Architecture of DeepGCGR

Fig. 1C illustrates the architecture of DeepGCGR, which consists of two layers of deep learning models. The P-model is designed to predict GCGR compound activity, while the C-model serves as a transfer learning model for GCGR compound classification. The P-model's architecture comprises a three-layer GAT network, which is then followed by global max pooling and a three-layer fully connected layer. In the C-model, a four-layer GCN network serves as a shared feature extractor, which is followed by a global max pooling layer. The resulting graph-level representations are then forwarded to a GCGR-specific classifica-

tion head composed of three fully connected layers, followed by a final output layer for prediction.

3.2. Evaluation of DeepGCGR

The training process for the P-model consisted of 200 epochs, with stabilization occurring around the 100th epoch (Fig. S1 A). The model's performance was evaluated using five-fold cross-validation, achieving MAE and MSE values below 0.5 and an R^2 up to 0.8. A correlation analysis between the predicted and actual values was shown in Fig. 2. The plots reveal a strong correlation, demonstrating that the model is well-suited for regression tasks. To further assess the efficacy of the P-model, we replaced the GAT layer with a GCN layer and compared their performance. We first visualized the results of both models across five-fold cross-validation using scatter plots (Fig. S2). The plots indicate that there is no significant difference between the two models, as both exhibit similar regression trends. We then performed a quantitative comparison. As shown in Table 2, the GAT-based model consistently outperformed the GCN-based model. While the difference was modest, it was consistent, suggesting that GAT provides a more accurate and reliable prediction of GCGR compound activity. Moreover, the P-model was also validated by using the dataset from Mizera et al. [29], which was employed to construct a QSAR model for GCGR activity prediction. The P-model demonstrated superior predictive performance, achieving a MAE of 0.4, which was better than the QSAR model's MAE of 0.44.

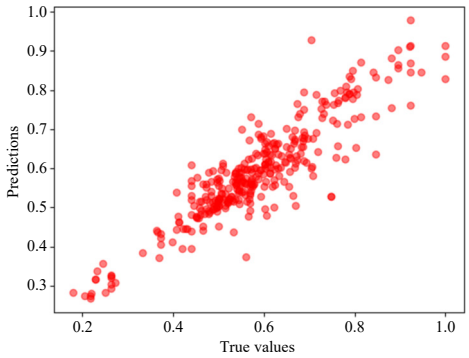

Fig. 2 Performance of the compound activity prediction model. The horizontal axis of the scatterplot represents the real values and the vertical axis represents the predicted values.

The training process for the C-model comprised both a pre-training and a fine-tuning stage. During pre-training, the model performance stabilized around the 170th epoch, with training terminating at the 198th epoch (Fig. S1 B). In the fine-tuning stage, stabilization occurred earlier, around the 40th epoch, with training concluding at the 95th epoch (Fig. S1 C). Throughout both stages, key performance metrics including ACC, F1 score, precision, and recall were tracked to monitor learning dynamics. As shown in Figs. S3 and S4, these metrics steadily improved and plateaued in later epochs. At the final evaluation, the model achieved an ACC of 0.98 and an F1 score of 0.99. For a comprehensive assessment of the C-model's predictive capability during fine-tuning, AUROC and AUPRC were plotted (Fig. 3). On the training set, the model's AUROC and AUPRC were 0.96 and 0.99, respectively. Its performance on the test set was even better, with both metrics reaching 0.99. Despite the imbalanced fine-tuning dataset (negative to positive sample ratio of 1 : 5), the C-model maintained strong predictive performance, demonstrating robust generalization and stability. To further illustrate classification performance on the imbalanced dataset, a confusion matrix was generated (Fig. S5), showing the distribution of true positives (TP), false positives (FP), true negatives (TN), and false negatives (FN), providing detailed insight into the model's accuracy in classifying compounds.

To investigate whether using GCN outperforms GAT, we compared the performance of the GCN-based model and the GAT-based model. Hence, we replaced the GCN layers with GAT layers and fine-tuned key hyperparameters of the GAT model, including the number of attention heads and the dropout rate. As shown in Table S2, incorporating the attention mechanism and tuning these parameters did not lead to significant performance improvements. This suggests that the GCN model is more suitable for classification tasks.

3.3. Interpretability analysis of the GCGR compound activity prediction model

To gain deeper insights into the chemical properties, types, and distribution of functional groups in the GCGR_P, we performed a comprehensive statistical analysis of key chemical characteristics. Various properties were calculated and analyzed, including the octanol-water partition coefficient (Log P) [40], molecular weight (MW), number of hydrogen bond donors (HBD), number of hydrogen bond acceptors (HBA), number of rotatable bonds (Rotatable Bonds), topological polar surface area (TPSA) [41], number of aliphatic rings (Aliphatic Ring), and number of nitrogen-containing aliphatic rings (Fig. S6).

The analysis revealed that the molecules in the P-model

Table 2 Performance comparison of the GCGR compound activity prediction models [a].

Fold number	Model	MSE	MAE	R^2
1	GCN	0.0051	0.0520	0.7724
	GAT	0.0050	0.0486	0.7774
2	GCN	0.0063	0.0578	0.7500
	GAT	0.0066	0.0580	0.7394
3	GCN	0.0053	0.0520	0.7515
	GAT	0.0044	0.0463	0.7934
4	GCN	0.0044	0.0464	0.7970
	GAT	0.0039	0.0454	0.8211
5	GCN	0.0040	0.0445	0.8099
	GAT	0.0040	0.0433	0.8126
Mean	GCN	0.0050 ± 0.0008	0.0505 ± 0.0047	0.7762 ± 0.0240
	GAT	0.0048 ± 0.0010	0.0483 ± 0.0051	0.7888 ± 0.0290

[a] MAE: mean absolute error; MSE: mean squared error.

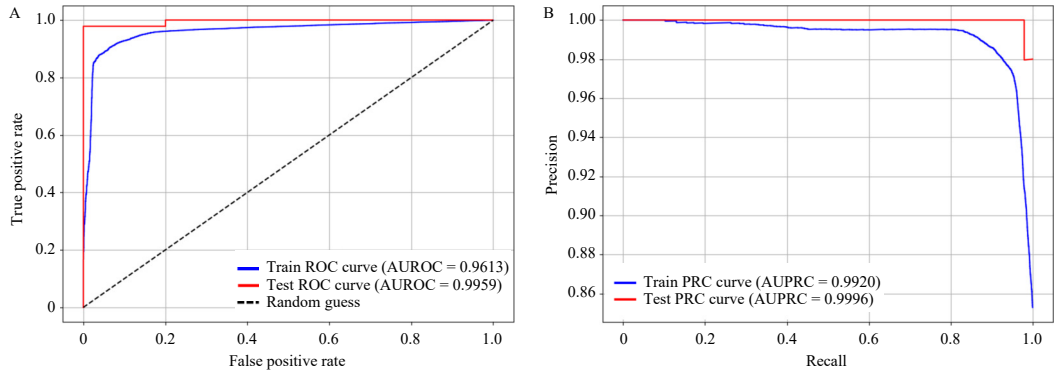

Fig. 3 Performance evaluation of the GCGR compound classification model. (A) Area under the ROC curves for the training and validation sets during the pre-training phase. (B) Precision-recall curves for the training and test sets during the fine-tuning phase.

training set generally conformed to Lipinski's rule of five [42], indicating favorable physicochemical properties indicative of drug-likeness. These molecules predominantly exhibited structural features such as nitrogen-containing aliphatic rings, aliphatic rings and halogen atoms. As reported in the literature, nitrogen-containing aliphatic rings are well-established pharmacophore elements commonly found in active small molecules targeting GPCRs [43]. In medicinal chemistry, fluorine and chlorine are frequently incorporated to improve a drug's ADME (absorption, distribution, metabolism, and excretion) profile, while bromine and iodine are generally employed to increase selectivity [44, 45]. For instance, Zhang et al. found that replacing hydrogen atoms with fluorine enhanced the binding affinity of compounds to their targets [46]. Furthermore, halogen atoms can facilitate protein-compound interactions by acting as halogen bond donors, hydrogen bond acceptors, or by participating in nonpolar interactions through π holes [47].

Based on the analysis of chemical properties, we selected two molecules with the highest and lowest IC_{50} values, along with two randomly selected molecules, to visualize attention weights. As shown in Fig. 4, the attention weight visualizations prominently highlight features such as nitrogen-containing aliphatic rings, aliphatic rings, and halogen atoms. These features align with established pharmacophore elements of active small molecules, supporting that the P-model can effectively identify critical pharmacophore components in small molecules targeting GCGR. In addition to the attention mechanism, we further employed SHAP (SHapley Additive exPlanations) [48] analysis to quantify the importance of molecular features. The top 20 most influential features, as ranked by their SHAP values, are summarized in a statistical plot (Fig. S7). In addition to atom type features, SHAP analysis further highlighted the role of other features during training, including the number of neighboring atoms attached to a given atom (Degree), the total number of explicit and implicit hydrogen atoms for atomic linkages (Hs), the implied electronic valence states of atoms (Valence), and whether an atom belongs to an aromatic ring system (Aromatic). These findings collectively indicate that the P-model's decision-making process is grounded in fundamental chemical and structural properties, providing an interpretable basis for its predictive performance.

3.4. Feature distribution visualization of the GCGR compound classification model

To visualize the spatial distribution of features at different stages of model training, we used t-distributed stochastic neighbor embedding (t-SNE). Features were examined before and after both pre-training and fine-tuning phases. The Davies-Bouldin Index (DBI) was used to quantitatively assess clustering quality, of-

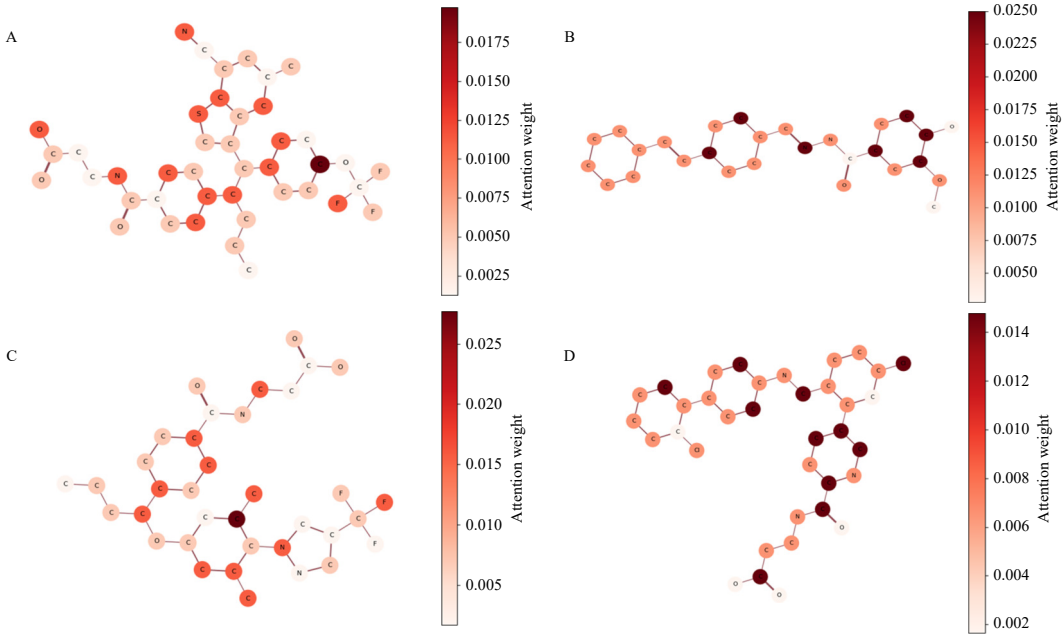

Fig. 4 Interpretability analysis based on attention score visualization. (A) Molecule with the smallest IC_{50}: CHEMBL3957356. (B) Molecule with the largest IC_{50}: CHEMBL431650. (C-D) Random molecule: CHEMBL2381847 and CHEMBL3675901. The darker color in the graph represents a higher attention score.

fering additional insight into the C-model's classification performance. As shown in Figs. 5A and 5B, the feature representations in the pre-training stage exhibited a disorganized distribution before training, with a DBI of 13.28. After training, the features became more compact and structured, and the DBI decreased to 3.74. Similarly, during fine-tuning (Figs. 5C and 5D), the DBI improved significantly from 5.83 before training to 0.35 after training, indicating enhanced clustering. These results demonstrate that both pre-training and fine-tuning stages progressively improve the model's ability to discriminate between GCGR agonists and antagonists through more distinct feature representations.

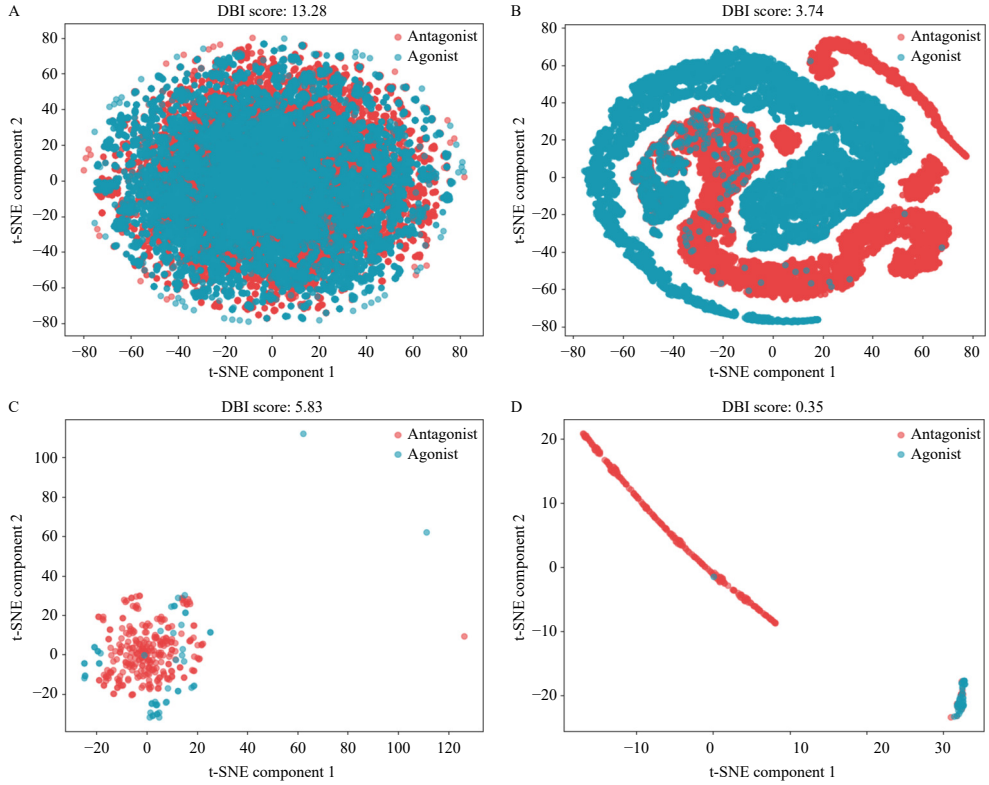

Fig. 5 Feature distribution analysis of the GCGR compound classification model. (A) Spatial distribution of the original features before pre-training. (B) Spatial distribution of the final-layer features after pre-training. (C) Spatial distribution of the original features before fine-tuning. (D) Spatial distribution of the final-layer features after fine-tuning.

3.5. Discovery of natural products with agonistic effects on GCGR

We applied the DeepGCGR model to virtually screen natural products derived from TCM for potential GCGR agonists targeting T2DM treatment. Initially, a natural products library consisting of 9 109 compounds was compiled from the TCM formulas used for T2DM treatment, which were obtained from the TCM knowledge discovery database (TCMKD, https://cbcb.cdutcm.edu.cn/TCMKD/) [49]. The P-model was then employed to predict the activity of these natural products against GCGR. As a result, 1 847 candidates with activity predicted values below 300 nmol·L^{-1} [50] were identified as high-activity GCGR compounds. These candidates were further refined by the C-model to 1 822 natural products with predicted agonistic effects. Subsequent molecular docking narrowed the selection to 1 065 compounds exhibiting docking scores below -7 kcal/mol, a threshold indicative of strong binding affinity [51]. The top 10 candidates ranked by their predicted activity values are illustrated in Fig. 6.

3.6. Functional validation of candidate natural products

To validate the virtual screening results, PMA (compound CID: 27924), a commercially available molecule from the top 10 candidates were selected for functional validation. The cAMP concentration-response curves of GCG were generated in the absence and presence of increasing concentrations of PMA. The addition of PMA induced a concentration-dependent enhancement of the cAMP response (Fig. 7A). Compared with the untreated control (normalized to 100%), Emax values of cAMP response increased to 125%, 150%, and 170% for the 0.1 μmol·L^{-1}, 1 μmol·L^{-1}, and 10 μmol·L^{-1} PMA-treated groups, respectively. This enhancement was primarily mediated by an increase in the maximum cAMP accumulation of GCG, with no significant change observed in the EC_{50} values, indicating that PMA may act as a positive allosteric modulator that increases the intrinsic efficacy of GCGR.

To investigate the molecular basis for this allosteric modulation, molecular docking was conducted to investigate the binding mode of PMA. Visualization using PyMOL (https://pymol.org/) revealed that PMA forms hydrogen bonds with key GCGR residues HIS-361 and GLN-392, located near the transmembrane domain (Fig. 7B). To further support this observation, the LogP of PMA was calculated using RDKit (http://www.rdkit.org/), yielding a value of 5.75, consistent with favorable binding within the hydrophobic transmembrane environment. These findings, together with the cAMP assay results, support the conclusion that PMA adopts a favorable binding conformation to enhance GCGR activation as a PAM.

4. Discussion

GCGR agonists have shown promising therapeutic potential for obesity and T2DM [14]. Natural products, with structural diversity and potential bioactivity, serve as an ideal reservoir for the discovery of GCGR-targeting agonists [52, 53]. However, traditional drug discovery methods often face challenges, including

CID: 12 544	CID: 322 885	CID: 21 968 638	CID: 5 320 469	CID: 439 520
Formula: C26H43NO5	Formula: C36H58O6	Formula: C30H46O7	Formula: C28H50O5	Formula: C24H4005
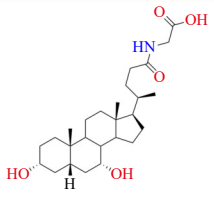	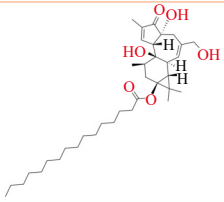	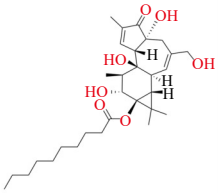	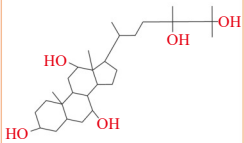	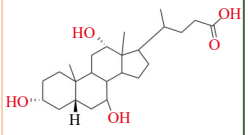
Binding affinity (kcal·mol^{-1}): −8.34	Binding affinity (kcal·mol^{-1}): −7.96	Binding affinity (kcal·mol^{-1}): −7.25	Binding affinity (kcal·mol^{-1}): −8.23	Binding affinity (kcal·mol^{-1}): −8.65
Predicted value (nmol·L^{-1}): 5.53	Predicted value (nmol·L^{-1}): 7.89	Predicted value (nmol·L^{-1}): 8.07	Predicted value (nmol·L^{-1}): 8.41	Predicted value (nmol·L^{-1}): 8.97
CID: 162 818 373	CID: 500 522	CID: 27 924	CID: 44 269 646	CID: 125 143
Formula: C29H48O4	Formula: C34H52O8	Formula: C36H56O8	Formula: C34H52O8	Formula: C29H50O2
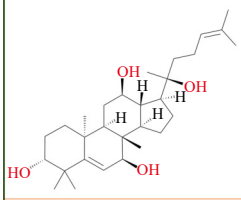	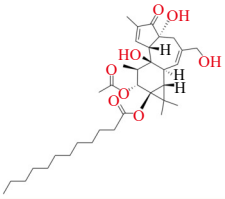	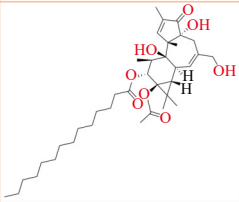	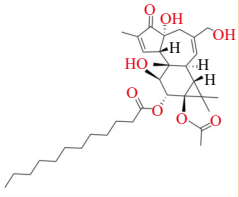	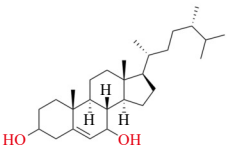
Binding affinity (kcal·mol^{-1}): −8.52	Binding affinity (kcal·mol^{-1}): −7.77	Binding affinity (kcal·mol^{-1}): −7.59	Binding affinity (kcal·mol^{-1}): −7.40	Binding affinity (kcal·mol^{-1}): −7.06
Predicted value (nmol·L^{-1}): 9.69	Predicted value (nmol·L^{-1}): 10.41	Predicted value (nmol·L^{-1}): 10.92	Predicted value (nmol·L^{-1}): 10.92	Predicted value (nmol·L^{-1}): 10.92

Fig. 6 Top ten compounds ranked by activity from virtual screening.

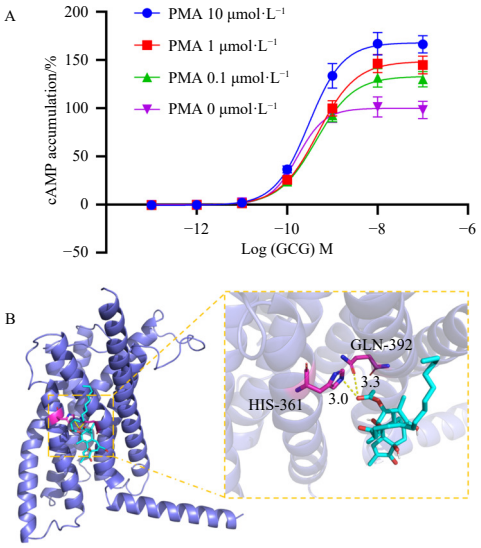

Fig. 7 Functional validation of natural products. (A) Effect of Phorbol 12-myristate 13-acetate (PMA) on glucagon-induced cAMP accumulation in HEK293T cells. Data are presented as mean ± standard deviation from three independent replicates. (B) Molecular docking visualization of PMA binding to GCGR. The GCGR structure is shown in blue-gray; PMA's carbon atoms are colored cyan, oxygen atoms in red, and hydrogen bonds are indicated by yellow dashed lines. Amino acid residues lining the binding pocket are depicted with purple carbons and blue nitrogens.

high costs and lengthy timelines [26]. To address these issues, we developed a two-layer deep learning model, DeepGCGR, to efficiently screen potential compounds with GCGR agonistic activity from a vast natural product library.

We constructed two datasets, GCGR_P for compound activity prediction and GCGR_C for compound classification, to train the P-model and C-model, respectively. The GCGR compound activity prediction model is based on the GAT. Its performance was evaluated using standard regression metrics, yielding a MAE and MSE below 0.5 and an R^2 of 0.8. Scatter plot analysis of predicted versus experimental activity values revealed a strong linear correlation, confirming the predictive accuracy of the model. For compound classification, we developed a GCGR-specific classification model (C-model) based on a graph convolutional network . Performance evaluation demonstrated that the C-model effectively addressed the inherent class imbalance in the dataset while maintaining high classification accuracy.

The statistical analysis of the P-model training set revealed that the molecules generally followed Lipinski's rule of five, indicating favorable drug-like properties. The molecules mainly featured nitrogen-containing aliphatic rings, aliphatic rings, and halogen atoms, which are known pharmacophore elements for active GPCR-targeting molecules. The attention weight visualizations, generated from selected molecules, highlight these key structural features, confirming that the P-model is capable of identifying critical pharmacophore elements in small molecules targeting GCGR.

By using DeepGCGR, we screened a library of 9 109 TCM-derived natural products and identified 1 065 candidates exhibiting GCGR agonism. This approach offers a substantial improvement over traditional methods, providing a more efficient and resource-conscious path toward novel T2DM therapeutics. Among the top-ranked candidates from virtual screening, PMA (compound CID: 27924), one of the top-ranked candidates from virtual screening, was selected for functional validation. Consistent with model predictions, PMA enhanced glucagon-induced cAMP responses in HEK293T cells in a concentration-dependent manner, supporting its role as a potential positive allosteric modulator of GCGR. While these findings provide encouraging initial evidence for the predictive power of DeepGCGR, additional functional assays involving diverse signaling pathways, and different cellular contexts will be required to further confirm the biological relevance and generalizability of the results.

Overall, DeepGCGR not only demonstrates the feasibility of leveraging deep learning for accurate prediction and classification of GCGR ligands but also marks an important advance in harnessing natural products as a valuable source of novel GCGR agonists. This integrative strategy may accelerate the discovery of next-generation therapeutics for T2DM and other GCGR-related diseases.

Acknowledgements

This work was supported by Natural Science Foundation of Sichuan (No. 2024ZDZX0019), National Natural Science Foundation of China (No. 32200576), the Innovation Team and Talents

Cultivation Program of National Administration of Traditional Chinese Medicine (No. ZYYCXTD-D-202408), and the talented person scientific research starts funds subsidization project of Chengdu University of Traditional Chinese Medicine (No.030040043 and No.030040017).

Declaration of competing interest

These authors have no conflict of interest to declare.

References

1 Ong KL, Stafford LK, McLaughlin SA, et al. Global, regional, and national burden of diabetes from 1990 to 2021, with projections of prevalence to 2050: a systematic analysis for the Global Burden of Disease Study 2021. *Lancet*. 2023;402(10397):203-234. https://doi.org/10.1016/S0140-6736(23)01301-6.

2 Jia YB, Liu Y, Feng LL, et al. Role of glucagon and its receptor in the pathogenesis of diabetes. *Front Endocrinol*. 2022;13:928016. https://doi.org/10.3389/fendo.2022.928016.

3 Chan JCN, Lim LL, Wareham NJ, et al. The Lancet Commission on diabetes: using data to transform diabetes care and patient lives. *Lancet*. 2021;396(10267):2019-2082. https://doi.org/10.1016/s0140-6736(20)32374-6.

4 Faselis C, Katsimardou A, Imprialos K, et al. Microvascular complications of type 2 diabetes mellitus. *Curr Vasc Pharmacol*. 2020;18(2):117-124. https://doi.org/10.2174/1570161117666190502103733.

5 Lv W, Wang XQ, Xu Q, et al. Mechanisms and characteristics of sulfonylureas and glinides. *Curr Top Med Chem*. 2020;20(1):37-56. https://doi.org/10.2174/1568026620666191224141617.

6 Qaseem A, Obley AJ, Shamliyan T, et al. Newer pharmacologic treatments in adults with type 2 diabetes: a clinical guideline from the American college of physicians. *Ann Intern Med*. 2024;177(5):658-666. https://doi.org/10.7326/m23-2788.

7 Zhao RC, Lu ZG, Yang J, et al. Drug delivery system in the treatment of diabetes mellitus. *Front Bioeng Biotechnol*. 2020;8:880. https://doi.org/10.3389/fbioe.2020.00880.

8 Rena G, Hardie DG, Pearson ER. The mechanisms of action of metformin. *Diabetologia*. 2017;60(9):1577-1585. https://doi.org/10.1007/s00125-017-4342-z.

9 Phua WWT, Wong MXY, Liao Z, et al. An aPPARent functional consequence in skeletal muscle physiology *via* peroxisome proliferator-activated receptors. *Int J Mol Sci*. 2018;19(5):1425. https://doi.org/10.3390/ijms19051425.

10 Feng JN, Jin T. Hepatic function of glucagon-like peptide-1 and its based diabetes drugs. *Med Rev*. 2024; 4(4): 312-325.https://doi.org/10.1515/mr-2024-0018.

11 Troke RC, Tan TM, Bloom SR. The future role of gut hormones in the treatment of obesity. *Ther Adv Chronic Dis*. 2014;5(1):4-14. https://doi.org/10.1177/2040622313506730.

12 Coskun T, Urva S, Roell WC, et al. LY3437943, a novel triple glucagon, GIP, and GLP-1 receptor agonist for glycemic control and weight loss: from discovery to clinical proof of concept. *Cell Metab*. 2022; 34(9): 1234-1247. e1239.https://doi.org/10.1016/j.cmet.2022.07.013.

13 Bossart M, Wagner M, Elvert R, et al. Effects on weight loss and glycemic control with SAR441255, a potent unimolecular peptide GLP-1/GIP/GCG receptor triagonist. *Cell Metab*. 2022; 34(1): 59-74. e10.https://doi.org/10.1016/j.cmet.2021.12.005.

14 Novikoff A, Müller TD. The molecular pharmacology of glucagon agonists in diabetes and obesity. *Peptides*. 2023;165:171003. https://doi.org/10.1016/j.peptides.2023.171003.

15 Sinha B, Ghosal S. Efficacy and safety of GLP-1 receptor agonists, dual agonists, and retatrutide for weight loss in adults with overweight or obesity: a bayesian NMA. *Obesity*. 2025.https://doi.org/10.1002/oby.24360.

16 Sánchez-Garrido MA, Brandt SJ, Clemmensen C, et al. GLP-1/glucagon receptor co-agonism for treatment of obesity. *Diabetologia*. 2017;60:1851-1861. https://doi.org/10.1007/s00125-017-4354-8.

17 Venugopal PP, Das BK, Soorya E, et al. Effect of hydrophobic and hydrogen bonding interactions on the potency of ß-alanine analogs of G-protein coupled glucagon receptor inhibitors. *Proteins*. 2020;88(2):327-344. https://doi.org/10.1002/prot.25807.

18 Varney MJ, Benovic JL. The role of G protein-coupled receptors and receptor kinases in pancreatic β-cell function and diabetes. *Pharmacol Rev*. 2024; 76(2):267-299. https://doi.org/10.1124/pharmrev.123.001015.

19 Kim T, Nason S, Antipenko J, et al. Hepatic mTORC2 signaling facilitates acute glucagon receptor enhancement of insulin-stimulated glucose homeostasis in mice. *Diabetes*. 2022;71(10):2123-2135. https://doi.org/10.2337/db21-1018.

20 Kim T, Holleman CL, Nason S, et al. Hepatic glucagon receptor signaling enhances insulin-stimulated glucose disposal in rodents. *Diabetes*. 2018;67(11):2157-2166. https://doi.org/10.2337/db18-0068.

21 Habegger KM. Cross talk between insulin and glucagon receptor signaling in the hepatocyte. *Diabetes*. 2022;71(9):1842-1851. https://doi.org/10.2337/dbi22-0002.

22 Laker RC, Egolf S, Will S, et al. GLP-1R/GCGR dual agonism dissipates hepatic steatosis to restore insulin sensitivity and rescue pancreatic β-cell function in obese male mice. *Nat Commun*. 2025;16(1):4714. https://doi.org/10.1038/s41467-025-59773-4.

23 Zhang ZH, Leng YL, Fu XX, et al. The efficacy and safety of dachaihu decoction in the treatment of type 2 diabetes mellitus: a systematic review and meta-analysis. *Front Pharmacol*. 2022;13:918681. https://doi.org/10.3389/fphar.2022.918681.

24 Bi ZH, Li H, Liang YT, et al. Emerging paradigms for target discovery of traditional medicines: a genome-wide pan-GPCR perspective. *The Innovation*. 2025;6(3):100774. https://doi.org/10.1016/j.xinn.2024.100774.

25 Rodrigues T, Reker D, Schneider P, et al. Counting on natural products for drug design. *Nat Chem*. 2016;8(6):531-541. https://doi.org/10.1038/nchem.2479.

26 Berdigaliyev N, Aljofan M. An overview of drug discovery and development. *Future Med Chem*. 2020;12(10):939-947. https://doi.org/10.4155/fmc-2019-0307.

27 Chen W, Liu XS, Zhang SY, et al. Artificial intelligence for drug discovery: resources, methods, and applications. *Mol Ther Nucl Acids*. 2023;31:691-702. https://doi.org/10.1016/j.omtn.2023.02.019.

28 Chen W, Song C, Leng L, et al. The application of artificial intelligence accelerates G protein-coupled receptor ligand discovery. *Engineering*. 2024;32:18-28. https://doi.org/10.1016/j.eng.2023.09.011.

29 Mizera M, Latek D. Ligand-receptor interactions and machine learning in GCGR and GLP-1R drug discovery. *Int J Mol Sci*. 2021;22(8):4060. https://doi.org/10.3390/ijms22084060.

30 Puszkarska AM, Taddese B, Revell J, et al. Machine learning designs new GCGR/GLP-1R dual agonists with enhanced biological potency. *Nat Chem*. 2024;16(9):1436-1444. https://doi.org/10.1038/s41557-024-01532-x.

31 Pándy-Szekeres G, Caroli J, Mamyrbekov A, et al. GPCRdb in 2023: state-specific structure models using AlphaFold2 and new ligand resources. *Nucleic Acids Res*. 2023;51(D1):D395-D402. https://doi.org/10.1093/nar/gkac1013.

32 Nguyen T, Le H, Quinn TP, et al. GraphDTA: predicting drug-target binding affinity with graph neural networks. *Bioinformatics*. 2021;37(8):1140-1147. https://doi.org/10.1093/bioinformatics/btaa921.

33 Nair V, Hinton GE. Rectified linear units improve restricted boltzmann machines. *ICML-10*. 2010;807–814. https://www.cs.toronto.edu/~fritz/absps/reluICML.pdf

34 Tang Q, Chen W. DeepB3P: a transformer-based model for identifying blood-brain barrier penetrating peptides with data augmentation using feedback GAN. *J Adv Res*. 2025;73:459-468.https://doi.org/10.1016/j.jare.2024.08.002.

35 Trott O, Olson AJ. AutoDock Vina: improving the speed and accuracy of docking with a new scoring function, efficient optimization, and multithreading. *J Comput Chem*. 2010;31(2):455-461. https://doi.org/10.1002/jcc.21334.

36 Siu FY, He M, de Graaf C, et al. Structure of the human glucagon class B G-protein-coupled receptor. *Nature*. 2013;499(7459):444-449. https://doi.org/10.1038/nature12393.

37 Berman HM, Westbrook J, Feng Z, et al. The protein data bank. *Nucleic Acids Res*. 2000;28(1):235-242. https://doi.org/10.1093/nar/28.1.235.

38 Kim S, Chen J, Cheng TJ, et al. PubChem in 2021: new data content and improved web interfaces. *Nucleic Acids Res*. 2021;49(D1):D1388-D1395. https://doi.org/10.1093/nar/gkaa971.

39 O'Boyle NM, Banck M, James CA, et al. Open Babel: an open chemical toolbox. *J Cheminf*. 2011;3:33. https://doi.org/10.1186/1758-2946-3-33.

40 Wildman SA, Crippen GM. Prediction of physicochemical parameters by atomic contributions. *J Chem Inf Comput Sci*. 1999;39(5):868-873. https://doi.org/10.1021/ci990307l.

41 Prasanna S, Doerksen RJ. Topological polar surface area: a useful descriptor in 2D-QSAR. *Curr Med Chem*. 2009;16(1):21-41. https://doi.org/10.2174/092986709787002817.

42 Lipinski CA. Drug-like properties and the causes of poor solubility and poor permeability. *J Pharmacol Toxicol Methods*. 2000;44(1):235-249. https://doi.org/10.1016/s1056-8719(00)00107-6.

43 Wang S, Che T, Levit A, et al. Structure of the D2 dopamine receptor bound to the atypical antipsychotic drug risperidone. *Nature*. 2018;555(7695):269-273. https://doi.org/10.1038/nature25758.

44 Gerebtzoff G, Li-Blatter X, Fischer H, et al. Halogenation of drugs enhances membrane binding and permeation. *Chembiochem*. 2004;5(5):676-684. https://doi.org/10.1002/cbic.200400017.

45 Gillis EP, Eastman KJ, Hill MD, et al. Applications of fluorine in medicinal chemistry. *J Med Chem*. 2015;58(21):8315-8359. https://doi.org/10.1021/acs.jmedchem.5b00258.

46 Zhang Q, Yin WH, Chen XY, et al. F-CPI: a multimodal deep learning approach for predicting compound bioactivity changes induced by fluorine substitution. *J Med Chem*. 2025: 706-718.https://doi.org/10.1021/acs.jmedchem.4c02668.

47 Shinada NK, de Brevern AG, Schmidtke P. Halogens in protein-ligand binding mechanism: a structural perspective. *J Med Chem*. 2019;62(21):9341-9356. https://doi.org/10.1021/acs.jmedchem.8b01453.

48 Lundberg SM, Lee SI. A unified approach to interpreting model predictions. *NeurIPS*. 2017; 30. https://proceedings.neurips.cc/paper/2017/file/8a20a8621978632d76c43dfd28b67767-Paper.pdf.

49 Xiao WK, Zhang MQ, Zhao DN, et al. TCMKD: from ancient wisdom to modern insights-A comprehensive platform for traditional Chinese medicine knowledge discovery. *J Pharm Anal*. 2025;15(6):101297. https://doi.org/10.1016/j.jpha.2025.101297.

50 Lenselink EB, Ten Dijke N, Bongers B, et al. Beyond the hype: deep neural networks outperform established methods using a ChEMBL bioactivity benchmark set. *J Cheminf*. 2017;9(1):45. https://doi.org/10.1186/s13321-017-0232-0.

51 Cao Y, Yao W, Yang T, et al. Elucidating the mechanisms of Buyang Huanwu Decoction in treating chronic cerebral ischemia: a combined approach using network pharmacology, molecular docking, and *in vivo* validation. *Phytomedicine*. 2024;132:155820. https://doi.org/10.1016/j.phymed.2024.155820.

52 Makhoba XH, Viegas C, Mosa RA, et al. Potential impact of the multi-target drug approach in the treatment of some complex diseases. *Drug Des Devel Ther*. 2020;14:3235-3249. https://doi.org/10.2147/dddt.S257494.

53 Chen W, Yu ZY, Leng L, et al. Artificial intelligence-curated repository of gene-encoded natural diverse components from herbal medicines. *The Innovation*. 2025;6:101011. https://doi.org/10.1016/j.xinn.2025.101011.